CrossMark

ORIGINAL PAPER

Simultaneous voltammetric determination of hydroquinone and catechol by using a glassy carbon electrode modified with carboxy-functionalized carbon nanotubes in a chitosan matrix and decorated with gold nanoparticles

Yu Shen[1,2] · Dejiang Rao[1] · Qinglin Sheng[1] · Jianbin Zheng[1]

Abstract The authors describe a method to anchor gold nanoparticles (AuNPs) on carboxy-functionalized multi-walled carbon nanotubes (c-MWCNTs) utilizing chitosan as dispersing and protective agent. A sensor for the simultaneous determination of hydroquinone and catechol was then fabricated by placing this nanocomposite on a glassy carbon electrode (GCE). The morphology and composition of the nanocomposites were characterized by scanning electron microscopy, transmission electron microscopy, energy-dispersive X-ray spectroscopy and X-ray powder diffraction. The electrochemical behavior of the modified GCE was studied by electrochemical impedance spectroscopy, cyclic voltammetry and differential pulse voltammetry. The modified GCE exhibits good electrooxidative activity towards hydroquinone and catechol and therefore was used for simultaneous determination of both, with typical voltages of 30 and 130 mV (vs. SCE). A linear reponse is found for the 0.5 μM to 1.5 mM hydroquinone concentration range, and for the 5.0 μM to 0.9 mM catechol concentration range. The respective lower detection limits are 0.17 and 0.89 μM (at an S/N ratio of 3). The sensitivity is 644.44 μA mM^{-1} cm^{-2} for hydroquinone and 770.98 μA mM^{-1} cm^{-2} for catechol.

Introduction

Hydroquinone (1,4-dihydroxybenzene, HQ) and catechol (1,2-dihydroxybenzene, CT), two isomers of the dihydroxybenzene, have been widely used in pharmaceutical industry, cosmetics manufacturing, rubber antioxidant, condiment field and other fields [1, 2]. As highly toxic organic compounds both for human health and environment, HQ and CT attract much attention on their sensitive and selective determination. Among many detection techniques such as chemiluminescence, capillary electrophoresis and high-performance liquid chromatography [3–6], non-enzymatic electrochemical detection is a potential and effective method for the simultaneous determination of HQ and CT because of its advantages of rapidity, sensitivity, stability and simplicity [7]. However, the overvoltages of their electrocatalytic oxidation and overlap between their oxidation peaks restrict the simultaneous electrochemical detection of HQ and CT [8]. Consequently, it is fascinating and challenging to establish a novel electrochemical method for their simultaneous determination.

Multi-walled carbon nanotubes (MWCNTs), considered as good catalyst template for the preparation of novel functional nanocomposites, have paved the approach for further construction of enhanced sensing platform for their particular characteristics [9]. However, the application of MWCNTs is limited by their low dispersion and aggregation among

✉ Qinglin Sheng
qinglinsheng@126.com

✉ Jianbin Zheng
zhengjb@nwu.edu.cn

[1] Institute of Analytical Science, Shaanxi Provincial Key Laboratory of Electroanalytical Chemistry, Northwest University, Xi'an, Shaanxi 710069, China

[2] Xi' an Northwest Geological Institute for Nonferrous Metals Co., Ltd., Xi' an, Shaanxi 710054, China

✆ Springer

individuals in aqueous solution [10]. To solve this problem, water-soluble groups, such as carboxylic acid groups, were introduced into MWCNTs' surface by continuous sonicate with a mixture of concentrated H_2SO_4 and HNO_3 [11]. Moreover, the carboxy-functionalized MWCNTs (c-MWCNTs) have been widely used in the construction of electrochemical sensors [12]. Zhai et al. reported an electrochemical sensor based on sulfonated graphene sheets and c-MWCNTs for the determination of clenbuterol, with a linear range of $1.0 \times 10^{-8} – 5.0 \times 10^{-6}$ mol L^{-1} and a low detection limit of 4.6×10^{-9} mol L^{-1} [13].

The introduction of nanomaterials such as gold nanoparticles (AuNPs) has been widely applied to the field of electrochemical sensing due to their good stability and remarkable conductivity [14–16]. Nevertheless, the aggregation between AuNPs severely affect their electrocatalytic performance for electroactive species [17]. To improve the dispersion of AuNPs, some dispersing and protective agents, such as polyvinylalcohol, poly(vinylpyrrolidone), Tween 20 and Chitosan (CTS), have been used during the formation of uniform morphology of AuNPs [18–20]. As a kind of natural polymer, CTS has been applied to the research of electrochemical sensing due to its advantages of multiple functional groups (amino groups and hydroxy groups) and film-forming properties [21]. The positively charged CTS film can be combined with negatively charged c-MWCNTs in aqueous solution under ultrasonic condition [22]. $AuCl_4^-$ can be largely adsorbed onto the surface of the positively charged CTS film, and then in-situ reduced by reductant to form AuNPs with high dispersion. Accordingly, we used chitosan as dispersing and protective agent to synthesize AuNPs anchored on the surface of CTS doped c-MWCNTs in our present study, which was feasible and novel.

Herein, a sensitive electrochemical sensor for simultaneous determination of HQ and CT was fabricated by a GCE modified with c-MWCNTs/CTS/Au nanocomposites which were synthesized with CTS as dispersing and protective agent. This nanocomposites can be further applied in the studies of materials science, optics and other electrochemical fields. The schematic illustration for the preparation of c-MWCNTs/CTS/Au nanocomposites (A) and c-MWCNTs/CTS/Au/GCE (B) are displayed in Scheme 1.

Experimental

Materials and Reagents

HQ, CT, phenol and resorcinol were supplied by Tianjin Kemiou Chemical Reagent Co., Ltd. (Tianjin, China, http://www.chemreagent.com/); Chloroauric acid tetrahydrate ($HAuCl_4 \cdot 4H_2O$, Purity >99.9%) was got from Shanghai Reagent Factory (Shanghai, China, http://shiyicr.company.lookchem.cn/); CTS (Molecular Weight: $5–6 \times 10^5$, Purity >90% deacetylation) was purchased from Shanghai Yuanju Biotechnology Co., Ltd. (Shanghai, China, http://www.yjbiotech.cn/); $NaBH_4$, HNO_3, $CuCl_2$ and H_2SO_4 were provided by Guangdong Guanghua Chemical Factory Co., Ltd. (Guangdong, China, http://www.jinhuada.com/); MWCNTs (Purity >95 wt%, Inside Diameter: 3–5 nm, Outer Diameter: 8–15 nm, Length < 50 μm) were obtained from Aladdin Industrial Corporation (Shanghai, China, http://www.aladdin-e.com/). The 0.1 mol L^{-1} phosphate buffered saline (PBS, pH 7.0) was employed in electrochemical investigations. The other reagents with analytical reagent grade were used in this study and the deionized water was

Scheme 1 The schematic illustration for the preparation of c-MWCNTs/CTS/Au nanocomposites (**a**) and c-MWCNTs/CTS/Au/GCE (**b**)
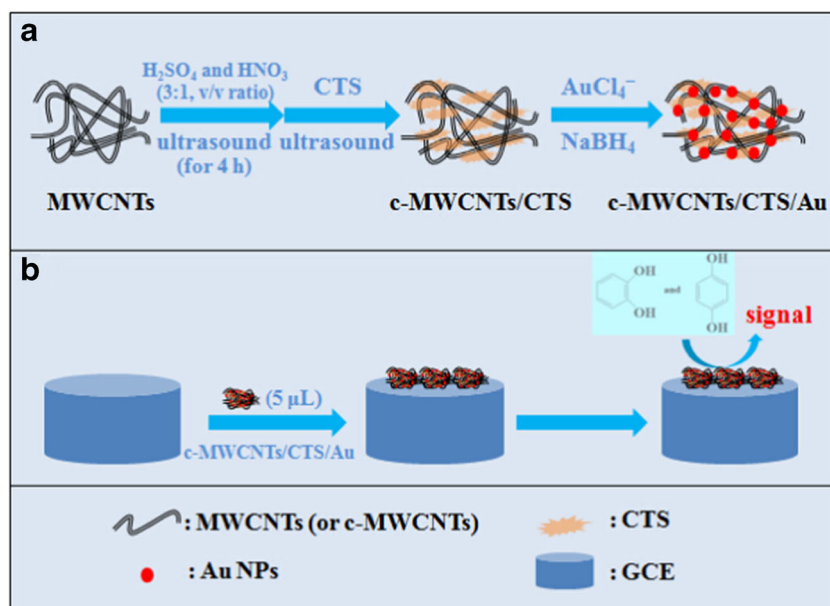
obtained by a Millipore system (Milli-Q, China, Resistivity >18 MΩ·cm, http://www.merckmillipore.com/CN/zh?bd=1) was used to prepare the aqueous solution.

Apparatus and Electrochemical Measurements

The transmission electron microscopy (TEM) was performed using a Tecnai G^2 F20 S-TWIN (FEI EIectron optics, USA) measurement operating at 200 kV. The images of scanning electron microscopy (SEM) and energy-dispersive X-ray spectroscopy (EDX) were acquired using a JSM-6700F (JEOL, Japan) measurement at operating voltage of 10 kV. The X-ray powder diffraction (XRD) datas were obtained using Cu Kα radiation at light tube power of 2.2 kW on a Bruker D8 Advance (Bruker AXS, Germany) measurement. The dynamic light scattering (DLS) experiments were performed on a particle size analyzer, model Zetasizer 1000HS (Malvern instruments, UK). The experiments of electrochemical impedance spectroscopy (EIS), cyclic voltammetry (CV) and differential pulse voltammetry (DPV) were carried out using a CHI 660D electrochemical workstation (Shanghai CH Instrument Co., Ltd., China) with a classic three-electrode system. Here, the bare GCE (diameter: 3.0 mm), c-MWCNTs modified GCE (c-MWCNTs/GCE), c-MWCNTs/CTS modified GCE (c-MWCNTs/CTS/GCE) and c-MWCNTs/CTS/Au modified GCE (c-MWCNTs/CTS/Au/GCE) were used as working electrodes, respectively. The Pt wire electrode and saturated calomel electrode (SCE) were used as counter electrode and reference electrode, respectively. All experiments were performed at room temperature (25 ± °C). The experimental parameters used for conducting EIS, DPV and CV experiments were specified in ESM.

Synthesis of c-MWCNTs/CTS composites

The c-MWCNTs were prepared following the procedure in ESM. The c-MWCNTs/CTS composites were prepared using a synthetic method reported by the literature with minor modifications [22]. In brief, 20 mg of c-MWCNTs was added into 20 mL of deionized water and completely dispersed by ultrasound to form a suspension (1.0 mg/mL). After that, 4 mL of CTS (0.5 wt%) was introduced into the above dispersion and kept continuous sonicate for 1 h. The black c-MWCNTs/CTS composites were collected by centrifugation at 6000 rpm with the relative centrifugational force of 3331g for 10 min, washed three times with deionized water and dried in an oven at 40 °C for 8 h.

Synthesis of c-MWCNTs/CTS/Au nanocomposites

The c-MWCNTs/CTS/Au nanocomposites were prepared by in-situ reduction. In a typical method, 10 mg of c-MWCNTs/CTS composites was thoroughly dispersed in deionized water (20 mL). Then, 0.4 mL of $HAuCl_4$ aqueous solution (1.0%, mass ratio) was introduced and kept in continuous ultrasound for 30 min. After that, excessive ice-cold $NaBH_4$ solution (1.2 mL of 10 mM) was subsequently added dropwise under stirring condition. This reaction was carried out at room temperature for another 1.5 h. The final products were collected by centrifugation at 6000 rpm with the relative centrifugational force of 3331g for 15 min, washed three times with deionized water and dried in air.

Modification of electrode

The GCE was polished to a mirror-like surface using 1.0 and 0.3 μm alumina slurries. The polished GCE was washed with deionized water, followed by ultrasound in a mixture solution of ethanol and water (1:1, v/v ratio). This GCE was dried in a stream of N_2. Then 1 mg of c-MWCNTs/CTS/Au nanocomposites were ultrasonically dispersed in 1 mL of deionized water. The suspension (5 μL) was painted onto the surface of GCE and dried in air at room temperature.

Results and discussion

Choice of Materials

MWCNTs, with high surface area, unique electrical and mechanical properties, can promote electron transfer between electrochemically active compounds and electrodes. The Hydrophilic c-MWCNTs can improve MWCNTs in synergistically electrocatalytic ability and adhesive ability, which make them favorable catalyst template for electrochemical sensors. In addition, CTS was used as dispersing and protective agent for its properties of film-forming ability, excellent adhesion and bridge cross linker. Moreover, the positively charged CTS film can be combined with negatively charged c-MWCNTs in aqueous solution under ultrasonic condition. To improve the stability and conductivity of the nanocomposites, AuNPs was introduced into the c-MWCNTs/CTS. $AuCl_4^-$ can be adsorbed onto the surface of the positively charged CTS film, and in-situ reduced into well dispersed AuNPs. Accordingly, we synthesize Au NPs anchored on the surface of CTS doped c-MWCNTs in our present study, and a sensitive electrochemical sensor for simultaneous determination of HQ and CT was fabricated by a GCE modified with c-MWCNTs/CTS/Au nanocomposites.

Optimization of method

The following parameters were optimized (Fig. S4B and C): (a) Sample pH value; (b) volume of $HAuCl_4$ solution. Respective data and Figures are given in the Electronic

Supporting Material. The following experimental conditions were found to give best results: (a) A sample pH value of 7.0; (b) A HAuCl$_4$ solution of 0.4 mL.

## Characterization of c-MWCNTs/CTS/Au Nanocomposites

Fig. S1 shows the SEM images of c-MWCNTs (A), c-MWCNTs/CTS composites (B) and c-MWCNTs/CTS/Au nanocomposites (C, D). As shown in Fig. S1A and B, the various-length c-MWCNTs with different orientation and the c-MWCNTs/CTS composites with compact network structure were clearly observed. Fig. S1C shows that many bright Au NPs were deposited on the surface of the c-MWCNTs/CTS composites. By further observation, in Fig. S1D it can be seen that the obtained Au NPs were uniformly anchored on the surface of compact network structure and without obvious aggregation.

The morphology of the nanocomposites was identified by TEM. Figure 1 displays the TEM images of c-MWCNTs (A), c-MWCNTs/CTS composites (B), c-MWCNTs/CTS/Au nanocomposites (C, D). As illustrated in Fig. 1a, the c-MWCNTs with typical tubular structures and smooth surface were clearly seen. Overall observation from Fig. 1b shows that the surface of the c-MWCNTs was covered by CTS films and no longer as smooth as before. It can be seen from Fig. 1c and

d that the well-dispersed AuNPs were near-spherical nanoparticles with a diameter of 12 ± 5 nm. Figure 1c shows a distribution of the synthesized AuNPs on the c-MWCNTs/CTS composites, suggesting c-MWCNTs/CTS/Au nanocomposites were successfully synthesized by this method of in-situ reduction. Fig. S2 is the Nanoparticles size deduced from DLS, which is in agreement with the size measured by TEM.

The composition of the c-MWCNTs/CTS/Au nanocomposites was studied by XRD and EDX. The XRD patterns of c-MWCNTs/CTS composites (A), c-MWCNTs/CTS/Au nanocomposites (B) and EDX pattern of c-MWCNTs/CTS/Au nanocomposites (C) are presented in Fig. 2. As shown in Fig. 2a, the sharp diffraction peak at 26.2° is attributed to the (002) plane of c-MWCNTs, while the peak at 44.5° is ascribed to the responds of iron contained impurities in c-MWCNTs samples [23, 24]. It can be demonstrated from the Fig. 2b that four obvious diffraction peak at 38.4, 44.6, 64.9 and 78.8° can be assigned to the (1 1 1), (2 0 0), (2 2 0) and (3 1 1) crystalline planes of face-centered cubic Au nanocrystals (JCPDS 4784), respectively [25, 26]. The EDX pattern of c-MWCNTs/CTS/Au nanocomposites (Fig. 2c) indicates that this nanocomposites are composed of C, O, N and Au elements. On the basis of characterization of SEM, TEM, XRD and EDX, it can be strongly proved that the c-MWCNTs/CTS/Au nanocomposites were successfully prepared by this synthesis method.

Fig. 1 TEM images of c-MWCNTs (**a**), c-MWCNTs/CTS composites (**b**), c-MWCNTs/CTS/Au nanocomposites (**c**, **d**)
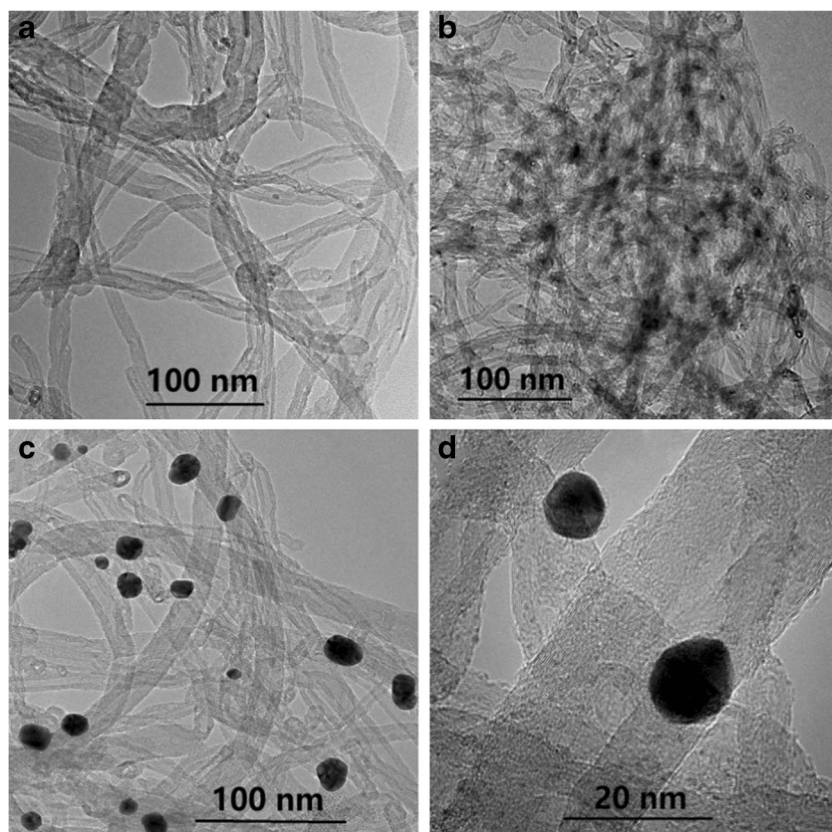
Fig. 2 XRD patterns of c-MWCNTs/CTS composites (**a**), c-MWCNTs/CTS/Au nanocomposites (**b**) and EDX pattern of c-MWCNTs/CTS/Au nanocomposites (**c**)
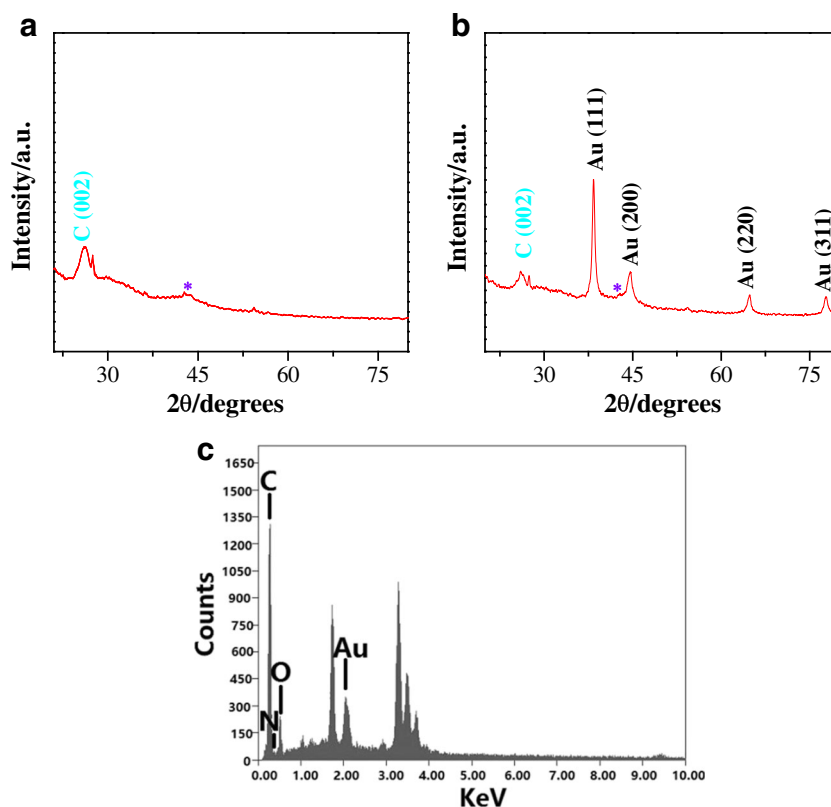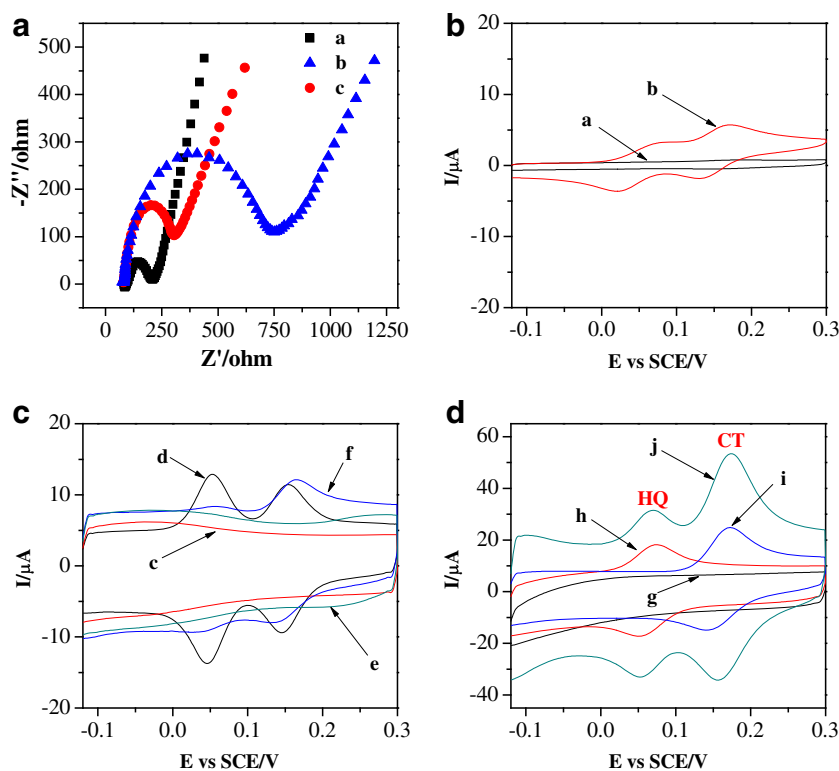

Electrochemical behavior of c-MWCNTs/CTS/Au nanocomposites

Electrochemical impedance spectroscopy (EIS) is a common method for investigating the electrical conductivity of surface modified electrodes. It is well-known that the semicircle diameter of Nyquist plots is equal to the electron transfer resistance (R_{et}) of electrodes [27], which can be affected by the conductivity and net charge of the modifying layers, and the electrostatic interactions between them and the probing species. Figure 3a displays the Nyquist plots of (a) the bare GCE, (b) c-MWCNTs/CTS/GCE and (c) c-MWCNTs/CTS/Au/GCE in 0.1 mol L^{-1} PBS (pH 7.0) containing 5.0 mM $[Fe(CN)_6]^{4-/3-}$ at open-circuit potential conditions with the AC amplitude of 5.0 mV. As shown in Fig. 3a, the bare GCE has an extremely small R_{et} value, and the values of R_{et} for different working electrodes were acquired in the following order: c-MWCNTs/CTS/GCE (639.5 Ω) > c-MWCNTs/CTS/Au/GCE (208.1 Ω) > GCE (127.4 Ω). The R_{et} value of c-MWCNTs/CTS/GCE is drastically decreased by 67.5% after the AuNPs were uniformly anchored on the surface of the c-MWCNTs/CTS composites. This phenomenon can be explained as follows: $[Fe(CN)_6]^{4-/3-}$ is a negatively charged redox probe, and the electron-transfer reaction involving $[Fe(CN)_6]^{4-/3-}$ at a negatively charged c-MWCNTs covering electrode surface will be blocked by the repulsive electrostatic forces. Moreover, the dispersing and protective agent chitosan

is not an excellent conductive material. Accordingly, although the c-MWCNTs/CTS composites have enlarged the electrode active surface area, the R_{et} of c-MWCNTs/CTS/GCE increased compared with bare GCE. The introduction of AuNPs can effectively improve the conductivity of the electrode and simultaneously accelerate the electron transfer rate at the solution/electrode interface, which decreases the R_{et} of c-MWCNTs/CTS/Au/GCE obviously.

Figure 3b and c show the CV curves of the bare GCE (a, b), c-MWCNTs/GCE (c, d) and c-MWCNTs/CTS/GCE (e, f) in 0.1 mol L^{-1} PBS (pH 7.0) in the absence (a, c and e) and presence (b, d and f) of HQ and CT (each 0.2 mM) at the scan rate (v) of 0.1 V s^{-1}. It's clear that all working electrodes show no obvious electrocatalytic response in the absence (a, c and e) of HQ and CT (each 0.2 mM) at the scan rate of 0.1 V s^{-1}. As can be seen in Fig. 3b, the bare GCE exhibits two pair of poor redox peaks with low peak currents in 0.1 mol L^{-1} PBS (pH 7.0) containing HQ and CT (each 0.2 mM). The electrochemical behavior on c-MWCNTs/CTS/GCE (e, f) is quite similar to that on the bare GCE. As shown in Fig. 3c, the c-MWCNTs/GCE displays two pair of well-defined redox peaks in 0.1 mol L^{-1} PBS (pH 7.0) containing 0.2 mM HQ and 0.2 mM CT. However, as shown in Fig. 3d, it is found that the c-MWCNTs/CTS/Au/GCE presents a pair of well-defined pedox peaks and an obvious increase of peak current responses (Fig. 3d) in 0.1 mol L^{-1} PBS (pH 7.0) in the presence of HQ and CT (each 0.2 mM) at the scan rate of 0.1 V s^{-1}. It can be

seen that two well-separated oxidation peaks were observed at
the anodic peak potential (E_{pa}) of 0.071 and 0.174 V, corre-
sponding to the electrocatalytic oxidation of HQ and CT on the
c-MWCNTs/CTS/Au/GCE, respectively. The anodic peak cur-
rent (I_{pa}) on the c-MWCNTs/CTS/Au/GCE increased by ap-
proximately double at least compared to c-MWCNTs/GCE
and c-MWCNTs/CTS/GCE. These results indicate that the c-
MWCNTs/CTS/Au/GCE is more efficient and presents en-
hanced electrocatalytic performance compared to that of the
c-MWCNTs/GCE. The AuNPs modified working electrode
can provide more electroactive sites and faster electron transfer
rate, all of which contribute to enhance the sensitivity of the
simultaneous determination of HQ and CT.

Fig. S4A illustrates the effect of pH value of 0.1 mol L^{-1} PBS
(pH: 5.0, 6.0, 7.0, 8.0 and 9.0) on the E_{pa} of c-MWCNTs/CTS/
Au/GCE in the presence of 0.2 mM HQ and 0.2 mM CT. As
shown in Fig. S4A, the E_{pa} shifted negatively and varied linearly
with the pH value of 0.1 mol L^{-1} PBS in the range from 5.0 to
9.0. The linear relation equation between E_{pa} and pH value were
evaluated to be E_{pa} (V) = 0.48–0.058 pH (r^2 = 0.9991) for HQ
and E_{pa} (V) = 0.60–0.061 pH (r^2 = 0.9995) for CT. According to
the following Nernst equation:

$$dEp/dpH = 2.303\ mRT/nF \tag{1}$$

Here, m is the number of proton, n is the number of elec-
tron, R is the gas constant, F is the Faraday constant and T is
the temperature in Kelvin [28]. In this study, m/n was

calculated to be 1.00 for HQ and 1.01 for CT in their electro-
catalytic oxidation reaction, and T is equal to 298.15 K.
Therefore, the slopes of the two linear equations we obtained
are approximately equal to the theoretical value of 0.059 V/
pH, indicating two protons and electrons involved in the elec-
trocatalytic process [29]. According to previous literatures, the
redox process of HQ and CT at a surface modified electrode is
a reversible process via the involvement of two electrons and
protons [8, 30]. The probable electrocatalytic mechanism of
HQ and CT at c-MWCNTs/CTS/Au/GCE is shown in Scheme
S1.

An electrochemical sensor was further investigated based
on the c-MWCNTs/CTS/Au nanocomposites since it presents
excellent electrocatalytic performance for simultaneous deter-
mination of HQ and CT. Figure 4a shows the CV curves of c-
MWCNTs/CTS/Au/GCE in 0.1 mol L^{-1} PBS (pH 7.0) in the
presence of different $C_{HQ} = C_{CT}$ ranging from 0.3 to 0.9 mM
in 0.1 mol L^{-1} PBS (pH 7.0) at a scan rate of 0.1 V s^{-1}. As
shown in Fig. 4a, two pair of well-defined redox peaks and
two well-separated oxidation peaks of HQ and CT were re-
corded. The I_{pa} and I_{pc} increased with the increase of
$C_{HQ} = C_{CT}$. Furthermore, it can be clearly seen that the I_{pa}
and I_{pc} of both HQ and CT with their concentrations exhibit
good linear relationship, as demonstrated in Fig. 4b and c,
suggesting a good suitability for simultaneous determination
of HQ and CT.

CV curves of HQ and CT (each 0.2 mM) in 0.1 mol L^{-1}
PBS (pH 7.0) at different scan rates in the range from 0.02 to

Fig. 4 CV curves obtained by c-MWCNTs/CTS/Au/GCE in 0.1 mol L^{-1} PBS (pH 7.0) in the presence of different $C_{HQ} = C_{CT}$ (From a to g: 0.3, 0.4, 0.5, 0.6, 0.7, 0.8 and 0.9 mM) in 0.1 mol L^{-1} PBS (pH 7.0) at a scan rate of 0.1 V s^{-1} (**a**); Linear fitting chart of I_{pa} and I_{pc} versus scan rate for HQ (**b**) and CT (**c**)
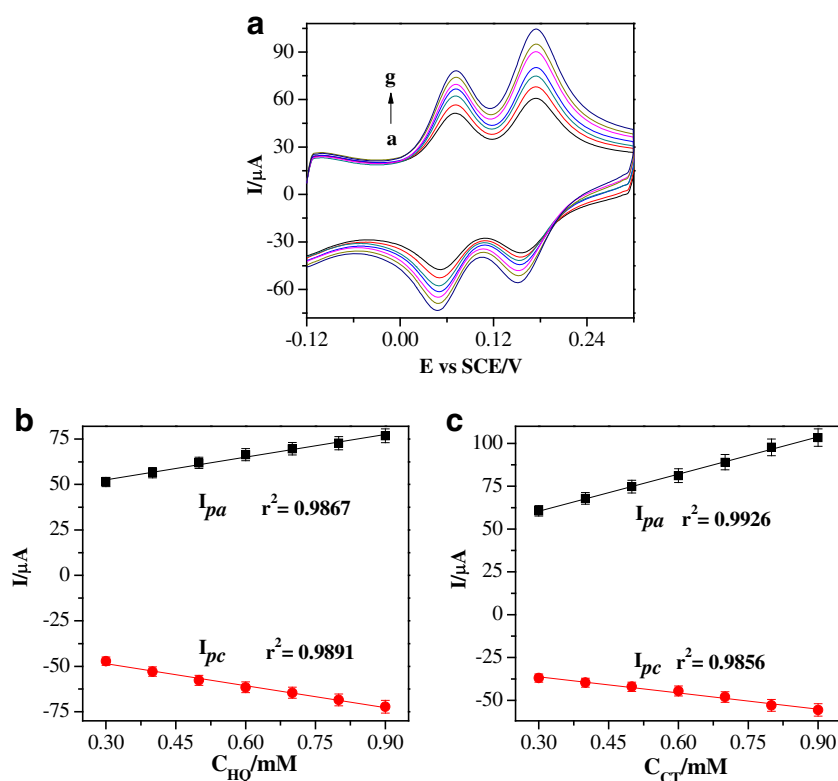
0.16 V·s^{-1} are shown in Fig. 5a. It can be found that the oxidation potentials of HQ and CT slightly shift in the positive direction. The oxidation and reduction peak currents of both HQ and CT increased with the raise of the scan rate. Figure 5b and c display the linear fitting chart of I_{pa} and I_{pc} versus v for HQ (B) and CT (C). As demonstrated in Fig. 5b and c, the I_{pa} and I_{pc} of both HQ and CT are linearly proportional to the v with good linear correlation coefficient. Therefore, the electrocatalytic behavior of both HQ and CT on the c-MWCNTs/CTS/Au/GCE is an adsorption-controlled process.

The electroanalytical performance of the c-MWCNTs/CTS/Au/GCE for simultaneous detection of HQ and CT was investigated by two different experiments. In each experiment, either the concentration of HQ or CT was just altered while maintaining other conditions remain unchanged. Figure 6a and b show the typical DPV curves of HQ with different concentrations in 0.1 mol L^{-1} PBS (pH 7.0) containing 0.1 mM CT (A) and the calibration plot constructed from the DPV responses for HQ (B). As illustrated in Fig. 6a, the I_{pa} of HQ at the potential of 30 mV (vs. SCE) increased with the increase of its concentration, while the I_{pa} and E_{pa} of CT keep obviously unchanged, suggesting no mutual interference was generated among the HQ and CT molecules. It can be observed from Fig. 6b that the I_{pa} of HQ was linear over the concentration range of $5.0 \times 10^{-7} - 1.5 \times 10^{-3}$ mol L^{-1} in the presence of 0.1 mM CT. Similarly, the DPV curves of CT with different concentrations in 0.1 mol L^{-1} PBS (pH 7.0) under the existence of 0.1 mM CT and the calibration plot

for HQ were shown in Fig. 6c and d. A calibration plot for CT in the concentration range of $5.0 \times 10^{-6} - 9.0 \times 10^{-4}$ mol L^{-1} was obtained with typical voltages 130 mV (vs. SCE), as shown Fig. 6d. The linear regression equations of this sensor were I_{pa} (μA) = 45.53 C_{HQ} (mM) + 5.62 (r^2 = 0.9994) with the sensitivity of 644.44 μA mM^{-1} cm^{-2} and I_{pa} (μA) = 54.47 C_{CT} (mM) + 6.97 (r^2 = 0.9984) with the sensitivity of 770.98 μA mM^{-1} cm^{-2} for HQ and CT, respectively. The detection limits (LOD) were calculated to be 0.17 μM for HQ and 0.89 μM for CT at the signal-to-noise ratio of 3 (S/N = 3).

Compared with the reported researches, our prepared sensor exhibits wider linear range and lower detection limit as well as higher sensitivity for the simultaneous detection of HQ and CT (Table 1). The possible reason is that c-MWCNTs provide a large number of active sites and AuNPs enhance the electron transfer rate effectively. Thus, this electrochemical sensor can be considered as an up-and-coming sensor for the sensitive and simultaneous detection of HQ and CT without mutual interference.

Reproducibility and Stability study

The reproducibility and stability of this c-MWCNTs/CTS/Au/GCE were carefully evaluated by DPV. Fig. S5 shows the reproducibility (A) and stability (B) of DPV responses for HQ and CT (each 0.2 mM) in 0.1 mol L^{-1} PBS (pH 7.0) at c-MWCNTs/CTS/Au/GCE. The reproducibility of five c-

Fig. 5 CV curves obtained by c-MWCNTs/CTS/Au/GCE in 0.1 mol L^{-1} PBS (pH 7.0) containing 0.2 mM HQ and 0.2 mM CT with different scan rates (From a to h: 0.02, 0.04, 0.06, 0.08, 0.10, 0.12, 0.14 and 0.16 V·s^{-1}) (**a**); Linear fitting chart of I_{pa} and I_{pc} versus v for HQ (**b**) and CT (**c**)
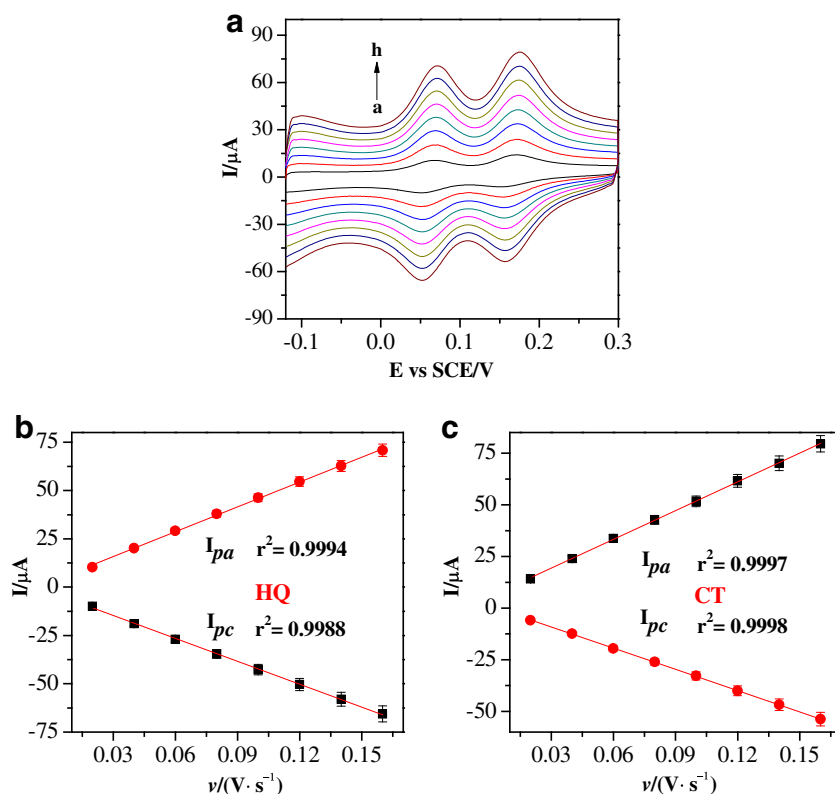
MWCNTs/CTS/Au/GCEs was evaluated by comparing the I_{pa} of HQ and CT (each 0.2 mM). The experimental results are shown in Fig. S5A. As demonstrated in Fig. S5A, the E_{pa} of

HQ and CT were not shifted obviously. Moreover, the relative standard deviation (RSD) of this reproducibility experiment is 3.21% for HQ and 4.13% for CT, demonstrating a good

Fig. 6 DPV curves of HQ with different concentrations in 0.1 mol L^{-1} PBS (pH 7.0) containing 0.1 mM HQ (**a**); DPV curves of CT with different concentrations (From a to n: 5, 7, 10, 30, 60, 100, 200, 300, 400, 500, 600, 700, 800, 900 and 1000 μM) in 0.1 mol L^{-1} PBS (pH 7.0) containing 0.1 mM CT (**c**); Calibration plots for HQ (**b**) and CT (**d**)
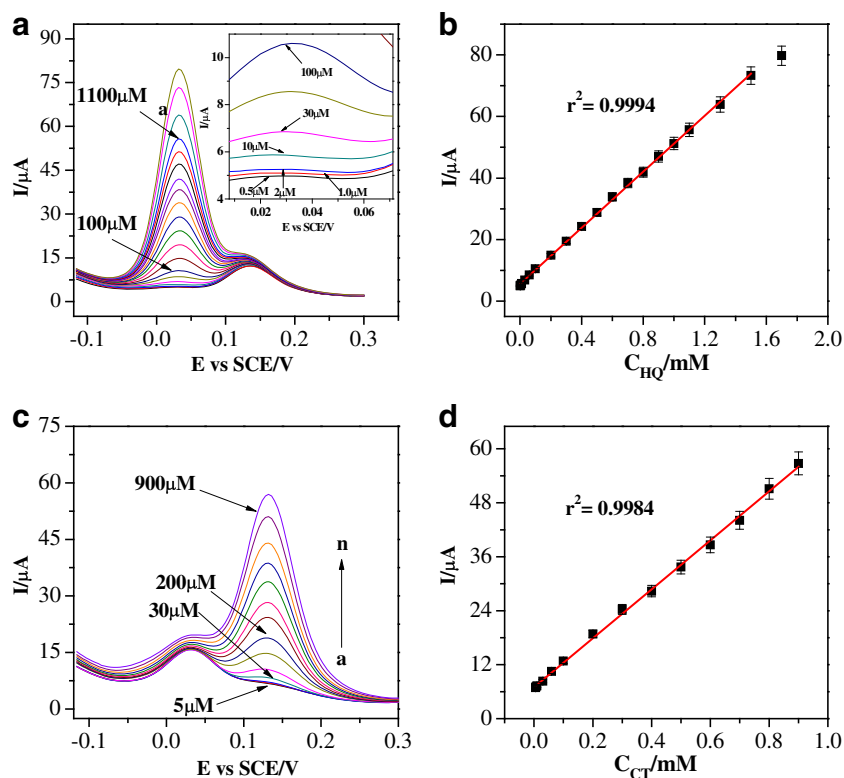
Table 1 Comparison of the sensing properties with other electrochemical sensors for the determination of HQ and CT

Sensors	Technology	pH	Linear range (μM)		LOD (μM)		Sensitivity (μA mM^{-1})		References
			HQ	CT	HQ	CT	HQ	CT	
PASA[a]/MWCNTs/GCE	DPV	6.0	6–100	6–180	1.0	1.0	14	24.48	[3]
MnO$_2$-Pt/GCE	DPV	7.0	3–481	15–447	–	–	27.2	18.1	[31]
(PEDOT/GO)[b]/GCE	DPV	6.0	2.5–200	2–400	1.6	1.6	–	–	[8]
p-Pen[c] modified GCE	DPV	5.0	15–115	25–175	0.6	1.0	1.57	1.06	[32]
LRG[d]/GCE	DPV	6.5	1–300	3–300	0.5	0.8	–	–	[29]
RGO[e]-MWCNTs/GCE	DPV	7.0	8–391	5.5–540	2.6	1.8	–	–	[33]
AgNPs[f]	CL[g]	–	–	–	0.1–10.0	–	0.005	–	–	[4]
CNF-Bi[h]/GCE	DPV	6.4	–	3–20	–	3–20	–	–	[34]
Au-G[i]/GCE	DPV	4.8	1–100	1–100	0.2	0.15	–	–	[35]
c-MWCNTs/CTS/Au/GCE	DPV	7.0	0.5–1500	5–900	0.17	0.89	45.53	54.47	This study

$^-$ not available;

[a] poly-amidosulfonic acid and multi-wall carbon nanotubes composite;

[b] graphene oxide doped poly(3,4-ethylenedioxythiophene);

[c] penicillamine;

[d] laser reduced graphene;

[e] reduced graphene oxide

[f] Silver nanoparticles

[g] Chemiluminescence

[h] Carbon nanofragments and bismuth oxide

[i] gold-graphene nanocomposite

reproducibility of the c-MWCNTs/CTS/Au/GCE. The experimental results of stability study are illustrated in Fig. S5B. We recorded the DPV responses (measure once a week) for HQ and CT (each 0.2 mM) in 0.1 mol L^{-1} PBS (pH 7.0) at c-MWCNTs/CTS/Au/GCE in a period of 3 weeks. The I_{pa} remained 89.3% for HQ and 90.5% for CT of its initial DPV responses after storage in a fridge for 3 weeks, indicating a good stability of the c-MWCNTs/CTS/Au/GCE.

Selectivity study

The selectivity of the c-MWCNTs/CTS/Au/GCE against possible interfering species was carefully examined by DPV. Some common ions and phenyl compounds, such as Ca^{2+}, Mg^{2+}, Na$^+$, Cu^{2+}, Hg^{2+}, Cl$^-$, NO^{3-}, SO$_4^{2-}$, CO$_3^{2-}$, nitrophenol, phenol and resorcinol were introduced into the 0.1 mol

L^{-1} PBS (pH 7.0) containing 0.05 mM HQ and 0.05 mM CT. It is worthy to note that these interfering species (each 5 mM) have no significant effect on the detection of HQ and CT. The DPV responses change below 4.5% after the addition of these interfering species, proving a good selectivity of our sensor.

Real sample analysis

To investigate the possible applicability and validity of the proposed method for the simultaneous determination of HQ and CC, laboratory tap water was tested without any pretreatment. Ten milliliters of tap water was diluted with 10 mL 0.1 M PBS (pH 7.0) for DPV measurement in the potential range of −0.12 and +0.3 V. HQ and CC were not found in the real samples, which meant that their contents were below the detection limits. Then the recovery experiment was utilized

Table 2 Recovery results for the determination of HQ and CT in the laboratory tap water samples ($n^* = 3$)

Sample number (NO.)	Added (μM)		Found (μM)		Recovery (%)		RSD (%)	
	HQ	CT	HQ	CT	HQ	CT	HQ	CT
NO. 1	8.0	8.0	8.2	8.3	102.5	103.8	3.2	2.8
NO. 2	36.0	36.0	35.4	36.5	98.3	101.4	2.9	3.1
NO. 3	136.0	136.0	137.8	135.1	101.3	99.3	3.5	2.4

*The result of average of three determinations by c-MWCNTs/CTS/Au/GCE

and the results were summarized in Table 2. The recoveries were in the range of 98.3–103.8% with the RSD below 3.5%, which clearly indicates the reliability of the proposed method.

Conclusions

In summary, the c-MWCNTs/CTS/Au nanocomposites were successfully synthesized by an attractive method utilizing chitosan as dispersing and protective agent. The DPV method was used to determine two dihydroxybenzene isomers (HQ and CT) simultaneously and quantitatively in a mixture. Based on the good electrochemical activity and electrical conductivity of the c-MWCNTs/CTS/Au/GCE, the detection of HQ and CC with good analytical performance was achieved with low detection limit, wide linear range, good selectivity, and significant sensitivity. To expand the application of the proposed method, it is necessary to conduct further research on improving the stability and durability of the modified electrode in our future work.

References

1. Xie TY, Liu QW, Shi YQ, Liu Q (2006) Simultaneous determination of positional isomers of benzenediols by capillary zone electrophoresis with square wave amperometric detection. J Chromatogr A 1109:317–321

2. Wang J, Park JN, Wei XY, Lee CW (2003) Room-temperature heterogeneous hydroxylation of phenol with hydrogen peroxide over Fe^{2+}, Co^{2+} ion-exchanged Naβ zeolite. Chem Commun 5: 628–629

3. Zhao DM, Zhang XH, Feng LJ, Jia L, Wang SF (2009) Simultaneous determination of hydroquinone and catechol at PASA/MWNTs composite film modified glassy carbon electrode. Colloids Surf B:Biointerfaces 74:317–321

4. Han SQ, Liu BB, Liu Y, Fan ZY (2016) Silver nanoparticle induced chemiluminescence of the hexacyanoferrate-fluorescein system, and its application to the determination of catechol. Microchim Acta 183(2):917–921

5. Guan N, Zeng ZR, Wang YC, Fu EQ, Cheng JK (2000) Open tubular capillary electrochromatography in fused-silica capillaries chemically bonded with macrocyclic dioxopolyamine. Anal Chim Acta 418:145–151

6. Marrubini G, Calleri E, Coccini T, Castoldi AF, Manzo L (2005) Direct analysis of phenol, catechol and hydroquinone in human urine by coupled-column HPLC with fluorimetric detection. Chromatographia 62:25–31

7. Zhang HS, Bo XJ, Guo LP (2015) Electrochemical preparation of porous graphene and its electrochemical application in the simultaneous determination of hydroquinone, catechol, and resorcinol. Sensors Actuators B Chem 220:919–926

8. Si WM, Lei W, Zhang YH, Xia MZ, Wang FY, Hao QL (2012) Electrodeposition of graphene oxide doped poly (3, 4-ethylenedioxythiophene) film and its electrochemical sensing of catechol and hydroquinone. Electrochim Acta 85:295–301

9. Han JF, Wang QQ, Zhai JF, Han L, Dong SJ (2015) An amperometric sensor for detection of tryptophan based on a pristine multi-walled carbon nanotube/graphene oxide hybrid. Analyst 140:5295–5300

10. Fresco-Cala B, Cárdenas S, Valcárcel M (2016) Improved microextraction of selected triazines using polymer monoliths modified with carboxylated multi-walled carbon nanotubes. Microchim Acta 183:465–474

11. Han Y, Zheng JB, Dong SY (2013) A novel nonenzymatic hydrogen peroxide sensor based on Ag-MnO$_2$-MWCNTs nanocomposites. Electrochim Acta 90:35–43

12. Yang JC, Wang X, Zhang DF, Wang LL, Li Q, Zhang L (2014) Simultaneous determination of endocrine disrupting compounds bisphenol F and bisphenol AF using carboxy functionalized multi-walled carbon nanotubes modified electrode. Talanta 130: 207–212

13. Zhai HY, Liu ZP, Chen ZG, Liang ZX, Su ZH, Wang SM (2015) A sensitive electrochemical sensor with sulfonated graphene sheets/oxygen-functionalized multi-walled carbon nanotubes modified electrode for the detection of clenbuterol. Sensors Actuators B Chem 210:483–490

14. Liu Z, Xu JK, Yue RR, Yang TT, Gao L (2016) Facile one-pot synthesis of Au–PEDOT/rGO nanocomposite for highly sensitive detection of caffeic acid in red wine sample. Electrochim Acta 196: 1–12

15. Gao YS, Xu JK, Lu LM, Zhu XF, Wang WM, Yang TT, Zhang KX, Yu YF (2015) A label-free electrochemical immunosensor for carcinoembryonic antigen detection on a graphene platform doped with poly(3, 4-ethylenedioxythiophene)/Au nanoparticles. RSC Adv 5(106):86910–86918

16. Gao YS, Zhu XF, Yang TT, Xu JK, Lu LM, Zhang KX (2015) Sensitive electrochemical determination of α-fetoprotein using a glassy carbon electrode modified with in-situ grown gold nanoparticles, graphene oxide and MWCNTs acting as signal amplifiers. Microchim Acta 182(11–12):2027–2035

17. Kannan P, Yoon CS, Yi SC, Lee SY, Kim DH (2015) Shape-controlled synthesis of gold-nickel bimetallic nanoparticles and their electrocatalytic properties. Mater Chem Phys 156:1–8

18. Dridi F, Marrakchi M, Gargouri M, Garcia-Cruz A, Dzyadevych S, Vocanson F, Saulnier J, Jaffrezic-Renault N, Lagarde F (2015) Thermolysin entrapped in a gold nanoparticles/polymer composite for direct and sensitive conductometric biosensing of ochratoxin A in olive oil. Sensors Actuators B Chem 221:480–490

19. Saengsookwaow C, Rangkupan R, Chailapakul O, Rodthongkum N (2016) Nitrogen-doped graphene-polyvinylpyrrolidone/gold nanoparticles modified electrode as a novel hydrazine sensor. Sensors Actuators B Chem 227:524–532

20. Du JJ, Wang ZK, Fan JL, Peng XJ (2015) Gold nanoparticle-based colorimetric detection of mercury ion via coordination chemistry. Sensors Actuators B Chem 212:481–486

21. Du Y, Luo XL, Xu JJ, Chen HY (2007) A simple method to fabricate a chitosan-gold nanoparticles film and its application in glucose biosensor. Bioelectrochemistry 70:342–347

22. Zhao G, Sun ZZ, Wang J, Xu Y, Muhammad F (2015) Development of biocompatible polymer actuator consisting of biopolymer chitosan, carbon nanotubes, and an ionic liquid. Polym Compos. doi:10.1002/pc.23728

23. Ahmadpoor F, Zebarjad SM, Janghorban K (2013) Decoration of multi-walled carbon nanotubes with silver nanoparticles and investigation on its colloid stability. Mater Chem Phys 139:113–117

24. Lorençon E, Ferreira DC, Resende RR, Krambrock K (2015) Amphiphilic gold nanoparticles supported on carbon nanotubes: Catalysts for the oxidation of lipophilic compounds by wet peroxide in biphasic systems. Appl Catal A Gen 505:566–574

25. Liu HY, Xu SH, He ZM, Deng AP, Zhu JJ (2013) Supersandwich cytosensor for selective and ultrasensitive detection of cancer cells using aptamer-DNA concatamer-quantum dots probes. Anal Chem 85:3385–3392

26. Yola ML, Atar N, Üstündağ Z, Solak AO (2013) A novel voltammetric sensor based on p-aminothiophenol functionalized graphene oxide/gold nanoparticles for determining quercetin in the presence of ascorbic acid. J Electroanal Chem 698:9–16

27. Mano N, Mao F, Heller A (2003) Characteristics of a miniature compartment-less glucose-O_2 biofuel cell and its operation in a living plant. J Am Chem Soc 125:6588–6594

28. Cano M, Rodríguez-Amaro R, Romero AJF (2008) Use of Butler-Volmer treatment to assess the capability of the voltammetric ion sensors: Application to a PPy/DBS film for cations detection. Electrochem Commun 10:190–194

29. Lai T, Cai WH, Dai WL, Ye JS (2014) Easy processing laser reduced graphene: A green and fast sensing platform for hydroquinone and catechol simultaneous determination. Electrochim Acta 138:48–55

30. Sanghavi BJ, Srivastava AK (2010) Simultaneous voltammetric determination of acetaminophen, aspirin and caffeine using an in situ surfactant-modified multiwalled carbon nanotube paste electrode. Electrochim Acta 55:8638–8648

31. Unnikrishnan B, Ru PL, Chen SM (2012) Electrochemically synthesized Pt-MnO_2 composite particles for simultaneous determination of catechol and hydroquinone. Sensors Actuators B Chem 169:235–242

32. Wang L, Huang PF, Bai JY, Wang HJ, Zhang LY, Zhao YQ (2007) Covalent modification of a glassy carbon electrode with penicillamine for simultaneous determination of hydroquinone and catechol. Microchim Acta 158:151–157

33. Hu FX, Chen SH, Wang CY, Yuan R, Yuan DH, Wang C (2012) Study on the application of reduced graphene oxide and multiwall carbon nanotubes hybrid materials for simultaneous determination of catechol, hydroquinone, p-cresol and nitrite. Anal Chim Acta 724:40–46

34. Liu LY, Ma Z, Zhu XH, Alshahrani LA, Tie SL, Nan JM (2016) A glassy carbon electrode modified with carbon nano-fragments and bismuth oxide for electrochemical analysis of trace catechol in the presence of high concentrations of hydroquinone. Microchim Acta 183(12):3293–3301

35. Ma XM, Liu ZN, Qiu CC, Chen T, Ma HY (2013) Simultaneous determination of hydroquinone and catechol based on glassy carbon electrode modified with gold-graphene nanocomposite. Microchim Acta 180(5–6):461–468